Progress In Electromagnetics Research, PIER 89, 225–253, 2009

THE ROLE OF THE IMPEDIVITY IN THE MAGNETOTELLURIC RESPONSE

R. Esposito and D. Patella

Department of Physical Sciences
University Federico II
Naples, Italy

Abstract—We study the influence of the resistivity frequency dispersion effects on the magnetotelluric (MT) response. Impedivity is the term used to indicate the frequency dependent resistivity in rocks. The impedivity functions, used in this paper, have been derived from the general solution of the motion equation of a charge carrier, discussed in a previous paper. A 1D three-layered earth section, with the second layer assumed to be dispersive, is considered to analyze the distortions due to dispersion on the modulus and phase of the MT responses on the earth's free surface. The MT responses of the section, where the dispersive layer is attributed an impedivity function describing at first a positive, then a negative and finally a resonant dispersion model, are computed for various combines of the dispersion parameters. A general conclusion is that the dispersion effects can strongly influence the MT response either in recognizable or in subtle forms. In the former case, the distortions appear as either steeply rising and/or descending curve branches or spike-like deltas, not compatible with a dispersion-free section. In the latter case, instead, the MT curves preserve the typical behavior for a dispersion-free section, and may thus erroneously be modeled by a section, where the dispersive layer is totally suppressed. In both case, disregarding the distortion effects may lead to misleading conclusions as to the physical properties of the surveyed structures.

Corresponding author: D. Patella (patella@na.infn.it).

1. INTRODUCTION

Resistivity dispersion is a known phenomenology [15, 31, 34], which in geophysics constitutes the basis of the Induced Polarization (IP) prospecting method [4, 11, 33, 36, 40]. In the frequency domain (FD), the dispersion consists in a variation of the resistivity parameter as the frequency of the exciting current is changed. The dispersive resistivity, called impedivity [24], is a complex function of the frequency. At vanishing frequency, however, the impedivity is real and coincides with the classical resistivity parameter used in DC geoelectrical methods. A real asymptote is also approached by the impedivity as the frequency tends to infinity.

So far, the IP FD spectrum in rocks has been modeled mostly using the Cole-Cole type impedivity function $\rho_+^{CC}(\omega)$ [5], given as

$$\rho_+^{CC}(\omega) = \rho_{+,0}\left[1 - m_+\frac{(i\omega\tau_+)^{c_+}}{1+(i\omega\tau_+)^{c_+}}\right], \tag{1}$$

which describes a typical positive dispersion model. In Eq. (1), $i = \sqrt{-1}$, ω is the angular frequency, $\rho_{+,0}$ is the DC resistivity and $m_+ \in [0,1]$, known in mining geophysics as chargeability, is the positive dispersion amplitude, defined as $m_+ = (\rho_{+,0} - \rho_{+,\infty})/\rho_{+,0}$, where $\rho_{+,\infty} \in [0, \rho_{+,0}]$ is the real impedivity at infinite frequency. Moreover, $c_+ \in [0,1]$ is the decay spectrum flatting factor and $\tau_+ \geq 0$ is the main time constant.

It has been shown that the electrical dispersion phenomenology can influence the magnetotelluric (MT) response in the typical $10^{-2} - 10^2$ Hz IP band [23, 35]. The detection and spatial definition of impedivity effects by MT can give a notable contribution to the understanding of the rock physical properties, well beyond the limited exploration depths of some tens m, reachable by the standard IP equipments.

Hydrocarbon and geothermal research are application fields, where MT is an ideal approach to detect dispersion-affected zones. These zones are fractured portions of rock, which have undergone diffuse alterations due to chemical interaction with uprising light hydrocarbons and hot fluids. These altered zones are considered reliable markers of the presence of exploitable reservoirs underneath.

Following the theory developed by [23, 24], the Cole-Cole model was included in MT to study the distortions provoked by dispersion on 1D [8] and 2D [19] synthetic responses. Positive dispersion effects in MT were experimentally recognized in volcanic and geothermal areas [6, 9, 10, 12, 20, 21, 27].

The aim of this paper is to further study the influence of the electric dispersion on MT, by analyzing the responses generated by the inclusion of negative and resonant dispersion models. These models have recently been proposed, with the aim of extending the application possibilities of the dispersion phenomenology in geophysics [25, 26].

2. THE GENERALISED DISPERSION MODEL

A generalized physical model was examined by [25], by solving in the FD the following electrodynamic equation of a charge carrier subject to an external electrical field $\mathbf{e}(\omega)$

$$\sum_{p=0}^{2} m_p (i\omega)^p \mathbf{r}(\omega) = q\mathbf{e}(\omega). \tag{2}$$

In Eq. (2), q and m_2 are the electrical charge and mass of the carrier, m_0 is an elastic-like parameter explaining recall effects, m_1 is a friction-like parameter accounting for dissipative losses due to collisions and $\mathbf{r}(\omega)$ is the Fourier transform of the trajectory of the charge.

Assuming, for simplicity, only one species of charge carriers and putting with K their number per unit of volume, the following elementary expression was derived for the impedivity $\rho(\omega)$ [25]

$$\rho(\omega) = \frac{m_0 + i\omega m_1 - \omega^2 m_2}{i\omega K q^2}. \tag{3}$$

Eq. (3) is a simple physical model, describing the behavior of a tuned circuit-like cell, i.e., a resistor–inductor–capacitor (RLC) series link. It is the equivalent of Lorentz's solution to the 2nd-order differential equation of harmonic oscillation [3].

2.1. The Positive Dispersion Model

By the generalized scheme reported above, a positive dispersion model was derived, assuming a dispersive rock equivalent to a serial chain of N two-branch parallel circuits. Each two-branch parallel circuit simulates the behavior of two different ionic species, which are both assumed to have negligible inertia, i.e., $m_{2,j}\omega^2 \approx 0$, where the index $j = 1, 2$ indicates the ionic species. One species ($j = 1$) is also assumed unbound, i.e., with $m_{0,1}$ negligible, and the other ($j = 2$) bound. In other words, one branch is a single R, in order to represent the path the unbound light ions can run through, with constant speed, under the action of an external exciting field. The other branch is, instead, an

RC series link, in order to represent the path the bound light ions can move through, under the action of the same external field and against the decelerating recall forces [25]. This assumption was proved to lead to the following dispersion formula [25, 26]

$$\rho_+^D(\omega) = \rho_{+,0}\left(1 - m_+ \sum_{n=1}^{N} \frac{i\omega\alpha_n}{1 + i\omega\tau_{+,n}}\right), \tag{4}$$

where $\rho_{+,0}$ and m_+ are the DC resistivity and the positive dispersion amplitude, as previously defined, and α_n and $\tau_{+,n}$ are related to the parameters K, q and m_p ($p = 0, 1, 2$) of each jth ($j = 1, 2$) species in each nth ($n = 1, \ldots, N$) two-branch parallel circuit, as reported in Table 1. They satisfy the condition $\sum_{n=1}^{N}(\alpha_n/\tau_{+,n}) = 1$ [25].

Table 1. Explicit formulae of the coefficients appearing in Eq. (4).

$\alpha_n = \dfrac{\sigma_{2,n}}{(\rho_{+,0} - \rho_{+,\infty})\gamma_{2,n}\sigma_{1,n}^2}$	$\rho_{+,0} = \sum_{n=1}^{N} \dfrac{1}{\sigma_{1,n}}$	$\rho_{+,\infty} = \sum_{n=1}^{N} \dfrac{1}{\sigma_{1,n} + \sigma_{2,n}}$
$\tau_{+,n} = \dfrac{\sigma_{1,n} + \sigma_{2,n}}{\gamma_{2,n}\sigma_{1,n}}$	$\sigma_{j,n} = \dfrac{K_{j,n}q_{j,n}^2}{(m_{1,j})_n}$ $(j{=}1{,}2)$	$\gamma_{2,n} = \dfrac{(m_{0,2})_n}{(m_{1,2})_n}$

Eq. (4) is an impedivity functions made of a discrete distribution of Debye dispersion terms [7]. This was the model almost exclusively used in the early IP works, notwithstanding the highest number of elementary terms often required to fit the experimental data. The Cole-Cole model reported in Eq. (1), originally considered an empirical law [41], was proved to be physically interpretable as a continuous distribution of Debye terms [30]. The Cole-Cole model has gained a widest popularity in geophysics, since the pioneering work by [29], thanks to the notably reduced number of unknown parameters, compared with the high number of parameters that characterize, instead, the discrete Debye distribution model.

2.2. The Negative Dispersion Model

By means of Eq. (3), [26] derived a new impedivity function, in order to fit less usual dispersion spectra showing a behavior opposite to that of the previous case [34]. It was argued that a dispersive rock can also be assimilated to a serial chain of N two-branch parallel circuits, each traveled by two distinct unbound ionic species, i.e., both with

negligible $m_{0,j}$ $(j = 1, 2)$. One species $(j = 1)$ was also assumed to have vanishing inertia, i.e., with $m_{2,1}\omega^2$ negligible. In other words, one branch was again a single R, representing, as previously, the path which the unbound light ions run through, with instantaneous constant speed, under the action of the external exciting field. The other branch was, instead, a RL link, in order to simulate the accelerated path the unbound heavy ions can travel through, subject to the same external field. The impedivity function thus obtained is featured by a discrete sum of Debye-type dispersion terms, as follows [26]

$$\rho_{-}^{D}(\omega) = \rho_{-,0}\left(1 - m_{-}\sum_{n=1}^{N}\frac{i\omega\beta_n}{1 + i\omega\tau_{-,n}}\right), \tag{5}$$

where $\rho_{-,0}$ is the DC resistivity and $m_{-} \in [-\infty, 0]$ is the negative dispersion amplitude, defined as $m_{-} = (\rho_{-,0} - \rho_{-,\infty})/\rho_{-,0}$. The coefficients β_n and $\tau_{-,n}$ are related to the parameters K, q and m_p $(p = 0, 1, 2)$ of each jth $(j = 1, 2)$ species in each nth $(n = 1, \ldots, N)$ two-branch circuit, as in Table 2. The condition $\sum_{n=1}^{N}(\beta_n/\tau_{-,n}) = 1$ is satisfied.

Table 2. Explicit formulae of the coefficients appearing in Eq. (5).

$\beta_n = \dfrac{\lambda_{2,n}\sigma_{2,n}}{(\rho_{-,0} - \rho_{-,\infty})(\sigma_{1,n} + \sigma_{2,n})^2}$	$\rho_{-,0} = \sum_{n=1}^{N}\dfrac{1}{\sigma_{1,n} + \sigma_{2,n}}$	$\rho_{-,\infty} = \sum_{n=1}^{N}\dfrac{1}{\sigma_{1,n}}$
$\tau_{-,n} = \dfrac{\lambda_{2,n}\sigma_{1,n}}{\sigma_{1,n} + \sigma_{2,n}}$	$\sigma_{j,n} = \dfrac{K_{j,n}q_{j,n}^2}{(m_{1,j})^2}$ $(j=1,2,3)$	$\lambda_{2,n} = \dfrac{(m_{2,2})_n}{(m_{1,2})_n}$

The formal identity between Eq. (4) and Eq. (5) allows the Cole-Cole formalism to be extended also to the negative dispersion as follows

$$\rho_{-}^{CC}(\omega) = \rho_{-,0}\left[1 - m_{-}\frac{(i\omega\tau_{-})^{c_{-}}}{1 + (i\omega\tau_{-})^{c_{-}}}\right], \tag{6}$$

where again $c_{-} \in [0, 1]$ is the decay spectrum flatting factor and $\tau_{-} \geq 0$ is the principal time constant. Noting that Eq. (5) for $N = 1$ and Eq. (6) for $c_{-} = 1$ become identical, it can easily be verified that also the $\rho_{-}^{CC}(\omega)$ function can physically be interpreted as a continuous distribution of Debye-type dispersion terms, following the procedure used by [30] for the positive dispersion.

2.3. The Resonant Dispersion Models

To avoid useless complications, in the following analysis devoted to the resonant assumption, we consider a system containing the least necessary number of distinct ionic species.

At first, we study the case of a system with only two distinct ionic species, where the first species ($j = 1$) is considered with negligible recall and inertia terms. An elementary cell of a dispersive rock is thus assumed to behave like a single two-branch parallel circuit, with a branch being a single R and the other an RLC series junction. The following elementary admittivity function corresponds with this model [26]

$$\sigma^{rf}(\omega) = \frac{1}{\rho_0} + \frac{i\omega\sigma_2}{\gamma_2 + i\omega - \omega^2\lambda_2}, \tag{7}$$

which represents a simple resonant flat (rf) dispersion model. The low-frequency and high-frequency admittivity asymptotes are now placed at the same level (flat asymptotic line), which means, in terms of resistivity, $\rho_0 = \rho_\infty$, i.e., a zero dispersion amplitude. The resonance effect occurs at $\omega = \sqrt{\gamma_2/\lambda_2}$. The parameters appearing in Eq. (7) are explicated in Table 3.

Table 3. Explicit formulae of the coefficients appearing in Eq. (7), Eq. (8) and Eq. (9).

$\sigma_j = \dfrac{K_j q_j^2}{(m_{1,j})^2}$ (j=1,2,3)	$\gamma_j = \dfrac{m_{0,j}}{m_{1,j}}$ (j=2,3)	$\lambda_j = \dfrac{m_{2,j}}{m_{1,j}}$ (j=2,3)

To conclude, we consider the resonance superimposed on either a positive or a negative dispersion effect. Therefore, we assume that the elementary cell now contains three different ionic species ($j = 1, 2, 3$) and behaves like a three-branch parallel circuit. The first branch is made of a single R ($j = 1$), the second branch of either a RC or a RL series link ($j = 2$), and the third branch by a RLC series combination ($j = 3$). The admittivity functions are [26]

$$\sigma^{r+}(\omega) = \frac{1}{\rho_{+,0}}\left[1 - m_+\frac{i\omega\tau_+}{1 + i\omega\tau_+}\right]^{-1} + \frac{i\omega\sigma_3}{\gamma_3 + i\omega - \omega^2\lambda_3}, \tag{8}$$

for the resonant positive (r^+) dispersion model, and

$$\sigma^{r-}(\omega) = \frac{1}{\rho_{-,0}}\left[1 - m_-\frac{i\omega\tau_-}{1 + i\omega\tau_-}\right]^{-1} + \frac{i\omega\sigma_3}{\gamma_3 + i\omega - \omega^2\lambda_3}, \tag{9}$$

for the resonant negative ($r-$) dispersion model. Both models resonate at $\omega = \sqrt{\gamma_3}/\lambda_3$. The explicit formulae of the new parameters appearing in Eq. (8) and Eq. (9) are given in Table 3.

The influence of the resonant positive dispersion on transient EM methods has been studied by [1, 37], who adopted the CC model given in Eq. (1), by arguing that for small chargeability values its validity can be extended to values of $c \in]1, 2[$ and that within this interval the resonance effects can be modeled.

3. THE MT RESPONSE IN PRESENCE OF DISPERSION

We show the results from a simulation of the MT responses, when the different dispersion models, separately, are assumed to characterize the electrical properties of a region of the explored half-space. A 1D three-layered earth, with its four A, Q, H, K type sections [14], is considered, with only the intermediate layer assumed to be dispersive. A fixed sequence of DC resistivities and thickness is attributed as in Fig. 1.

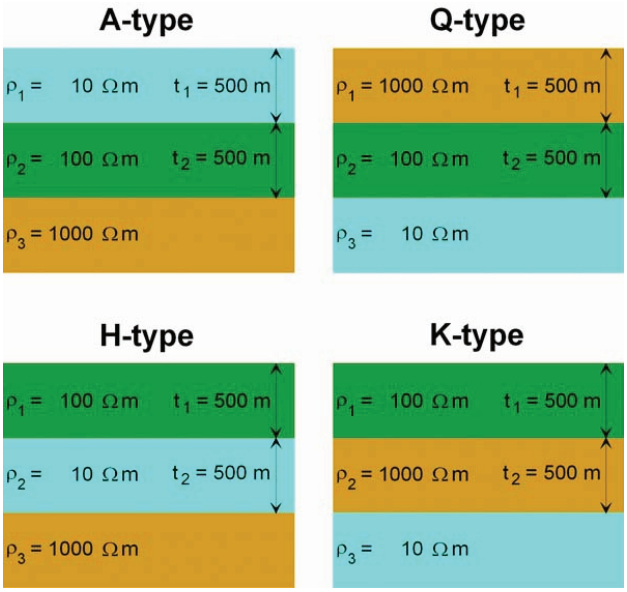

Figure 1. The three-layer A, Q, H and K type sections used for all of the dispersive MT simulations.

The formula used to extract modulus and phase of the MT complex response at the earth surface, i.e., the apparent impedivity

function $\rho_a^d(\omega)$, for the three-layer earth with a dispersive intermediate layer is given as [24]

$$\rho_a^d(\omega) = \rho_1 \mathrm{th}^2 \left\{ k_1 t_1 + \mathrm{th}^{-1} \left[\sqrt{\frac{\rho_2(\omega)}{\rho_1}} \mathrm{th} \left(k_2 t_2 + \mathrm{th}^{-1} \sqrt{\frac{\rho_3}{\rho_2(\omega)}} \right) \right] \right\}, \quad (10)$$

where t_1 and t_2 are the thickness of the 1st and 2nd layer, respectively, ρ_1 is the DC resistivity of the 1st layer and ρ_3 that of the substratum, and th stands for hyperbolic tangent. Moreover k_1 and k_2 are the wavenumbers in the 1st and 2nd layer, given by $k_1 = \sqrt{(i\omega\mu_o/\rho_1)}$ and $k_2 = \sqrt{[i\omega\mu_o/\rho_2(\omega)]}$, respectively, being μ_o the magnetic permeability of free space, equal to $4\pi \cdot 10^{-7}$ H/m in SI units, used throughout the paper. The impedivity $\rho_2(\omega)$ of the second layer is given, separately, the expressions in Eqs. (1) and (6), and the inverse of the expressions in Eqs. (7), (8) and (9). The thickness and DC resistivity values attributed to the layers are reported in Fig. 1.

In all of the sets of diagrams which will be shown, the reference not dispersive MT response will always be drawn for comparison. Moreover, for each dispersion law, only a few simulations will be drawn, sufficient to deduce the relevant aspects of the dependence of the MT response on the dispersion parameters. It must be pointed out that the MT phase curves that will be shown describe the behavior of the phase of the apparent impedivity function defined in eq. (10). This a slightly different representation compared with that used in classical not dispersive MT, where the phase curves of the wave impedance are generally drawn, e.g., [42]. Using the well known relationship between apparent impedivity and wave impedance, e.g., [19, 24, 42], it can be easily demonstrated that the apparent impedivity phase function is equal to two times the impedance phase function minus 90°.

3.1. The MT Response with Non-resonant Positive Dispersion

Referring to the Cole-Cole dispersion model in Eq. (1), based on the three dispersion parameters c_+, m_+ and τ_+, the simulations have been done by fixing two of them and letting the third vary. The following three sets of simulations have thus been computed:

1st set: $c_+ = 0.75$, $m_+ = 0.9$ and $\tau_+ = 1$, 10, 100 s, (Fig. 2(a)),

2nd set: $m_+ = 0.9$, $\tau_+ = 100$ s and $c_+ = 0.25$, 0.5, 0.75, (Fig. 2(b)),

3rd set: $c_+ = 0.75$, $\tau_+ = 100$ s and $m_+ = 0.1$, 0.5, 0.9, (Fig. 2(c)).

Figure 2(a) shows that the dispersion phenomenology provokes a very limited effect on the curves belonging to the A, Q and K three-

layer sections. Conversely, for the H type section a magnificent effect is visible on both the modulus and phase dispersive curves, substantially diverging from the reference dispersion-free MT curves. However, the influence the main time constant τ_+ has on distorting the curves is quite imperceptible for all of the type sections, though τ_+ has been let to vary by two orders of magnitude from 1 s to 100 s. In fact, the blue

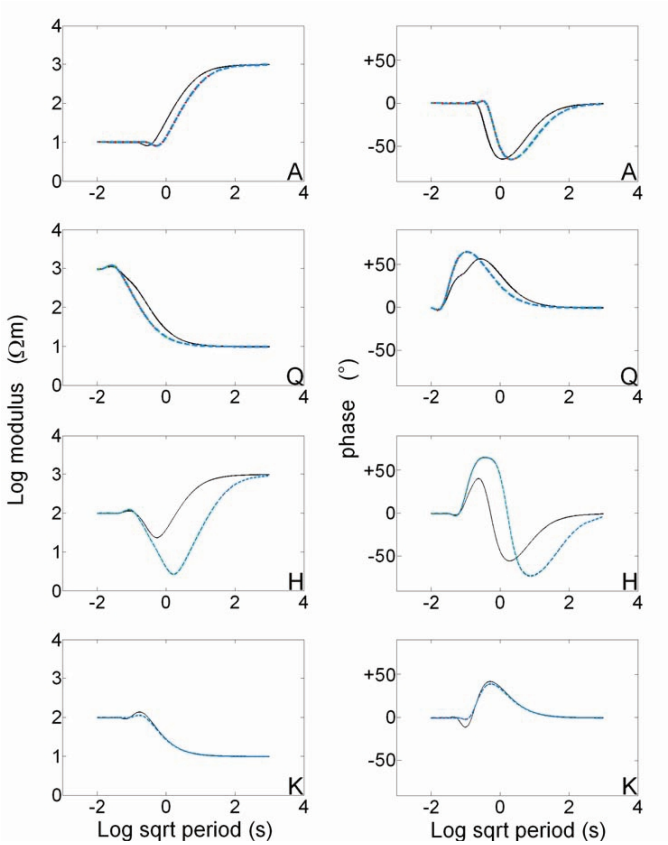

Figure 2a. MT apparent impedivity modulus and phase simulated responses for the A, Q, H and K three-layer sequences of Fig. 1, with the second layer affected by a Cole-Cole type non-resonant positive dispersion. The black lines are the reference not dispersive MT responses. The positive dispersion amplitude and flatting factor are fixed, respectively $m_+ = 0.9$ and $c_+ = 0.75$, while the principal time constant is variable with values $\tau_+ = 1$ s (red line), $\tau_+ = 10$ s (green line) and $\tau_+ = 100$ s (blue line).

curves, corresponding to the highest τ_+ value, wholly absorb the nearly coincident red and green curves, corresponding to the lower values of τ_+.

Figure 2(b) shows that also the influence of the flatting factor c_+ is quite limited, but a little more evident than in the former case. The red curves, corresponding to the lowest c_+ can be distinguished from

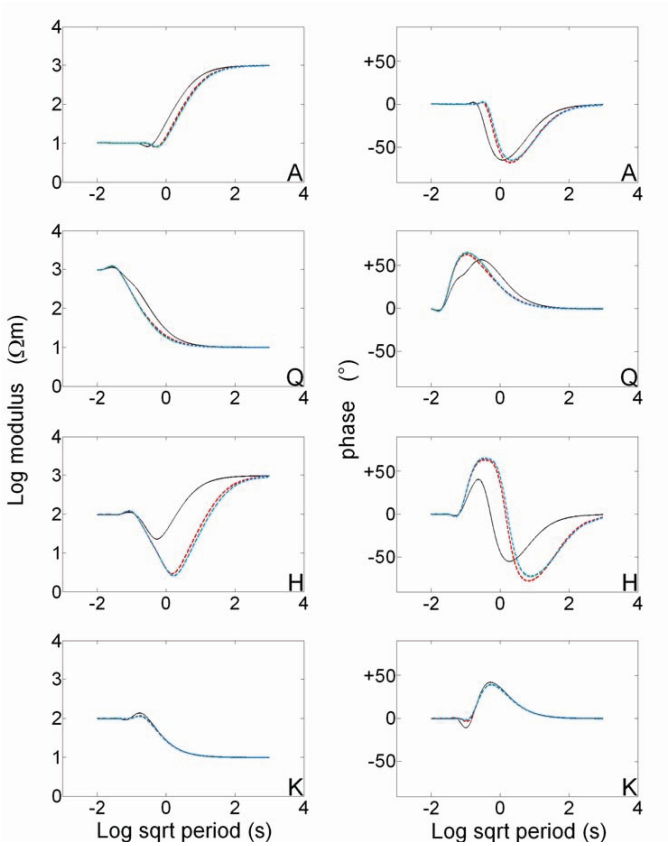

Figure 2b. MT apparent impedivity modulus and phase simulated responses for the A, Q, H and K three-layer sequences of Fig. 1, with the second layer affected by a Cole-Cole type non-resonant positive dispersion. The black lines are the reference not dispersive MT responses. The positive dispersion amplitude and principal time constant are fixed, respectively $m_+ = 0.9$ and $\tau_+ = 100\,\mathrm{s}$, while the flatting factor is variable with values $c_+ = 0.25$ (red lines), c_+=0.5 (green lines) and $c_+ = 0.75$ (blue lines).

the blue curves, corresponding to the highest c_+. Again, the dispersion phenomenon has a poor influence on the curves belonging to the A, Q and K type sections. Conversely, for the H type section a magnificent effect is again visible on both the modulus and phase dispersive curves. The evidence that the H section is the most responsive to the influence of dispersion may have a notable impact on the interpretation of MT

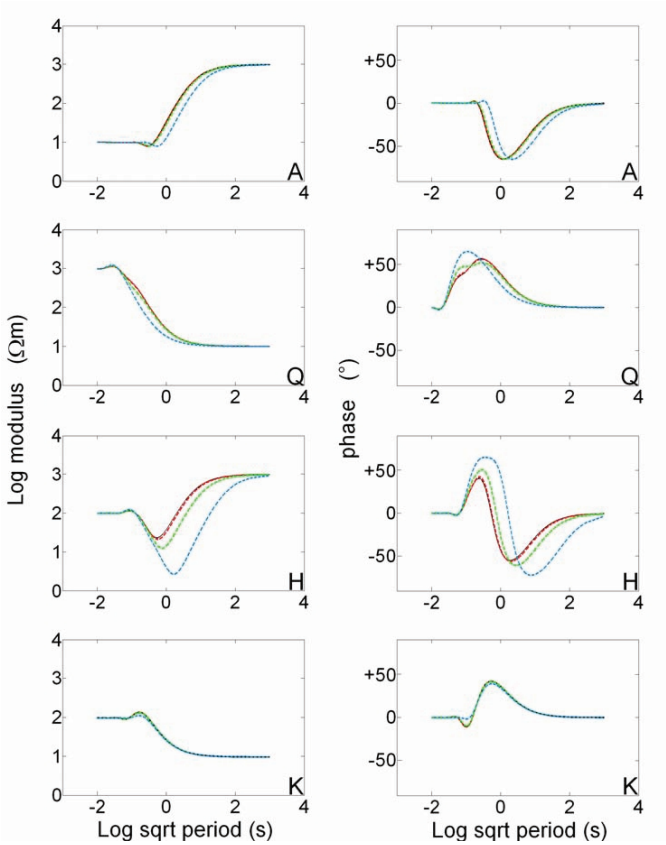

Figure 2c. MT apparent impedivity modulus and phase simulated responses for the A, Q, H and K three-layer sequences of Fig. 1, with the second layer affected by a Cole-Cole type non-resonant positive dispersion. The black lines are the reference not dispersive MT responses. The flatting factor and principal time constant are fixed, respectively $c_+ = 0.75$ and $\tau_+ = 100\,\mathrm{s}$, while the positive dispersion amplitude is variable with values $m_+ = 0.1$ (red lines), $m_+ = 0.5$ (green lines) and $m_+ = 0.9$ (blue lines).

data. In fact, in the application fields mentioned in the introduction, i.e., oil and geothermal exploration, the H section is by far the most representative earth model. This aspect will be further discussed in the next section after the presentation of all of the dispersion typologies.

Finally, Fig. 2(c) shows the positive dispersion amplitude m_+ as widely influencing the shape of the dispersive responses. In fact, a large

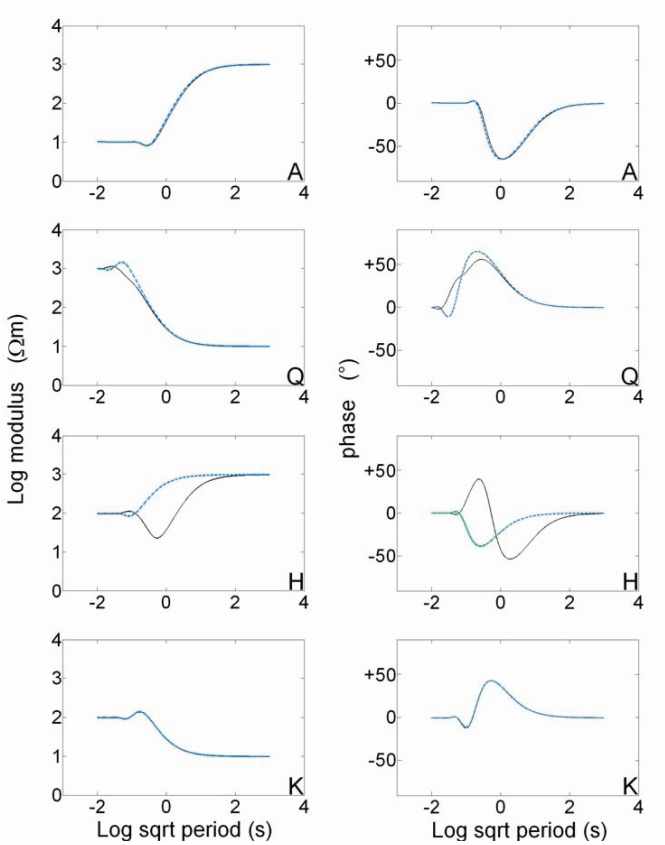

Figure 3a. MT apparent impedivity modulus and phase simulated responses for the A, Q, H and K three-layer sequences of Fig. 1, with the second layer affected by a Cole-Cole type non-resonant negative dispersion. The black lines are the reference not dispersive MT responses. The negative dispersion amplitude and flatting factor are fixed, respectively $m_- = -999$ and $c_- = 0.75$, while the principal time constant is variable with values $\tau_- = 1\,\mathrm{s}$ (red lines), $\tau_- = 10\,\mathrm{s}$ (green lines) and $\tau_- = 100\,\mathrm{s}$ (blue lines).

spread appears from the red curves, corresponding with the lowest value of m_+, which nearly coincide with the dispersion-free curves, to the blue curves, corresponding with the highest value of m_+.

Practically, all of these simulations show what it was expected, i.e., that the dispersion alters the shape of the curves in the same way as a lowering of the DC resistivity of the second layer

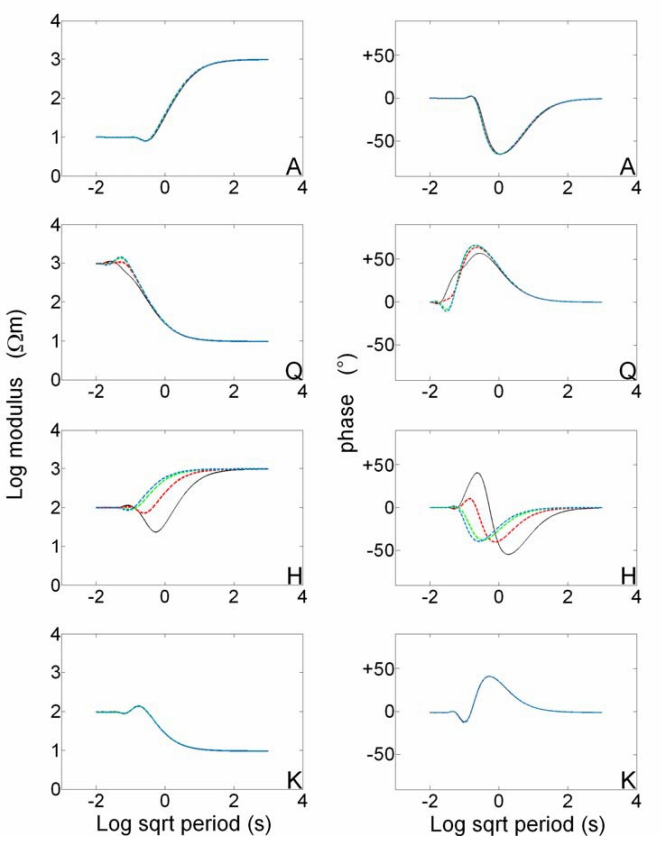

Figure 3b. MT apparent impedivity modulus and phase simulated responses for the A, Q, H and K three-layer sequences of Fig. 1, with the second layer affected by a Cole-Cole type non-resonant negative dispersion. The black lines are the reference not dispersive MT responses. The negative dispersion amplitude and principal time constant are fixed, respectively $m_- = -999$ and $\tau_- = 100\,\mathrm{s}$, while the flatting factor is variable with values $c_- = 0.25$ (red lines), $c_- = 0.5$ (green lines) and $c_- = 0.75$ (blue lines).

does in a not dispersive situation. Such equivalence, without any external constraints, may make the interpretation of the curves quite ambiguous, as far as the maximum permitted slopes for dispersion-free curves are not surpassed. Of course, by this limited analysis, no general rule can be drawn as to the way the MT curves will be distorted by changing the dispersion parameters. The distortion will basically depend on how large is the frequency window of the MT waves fading

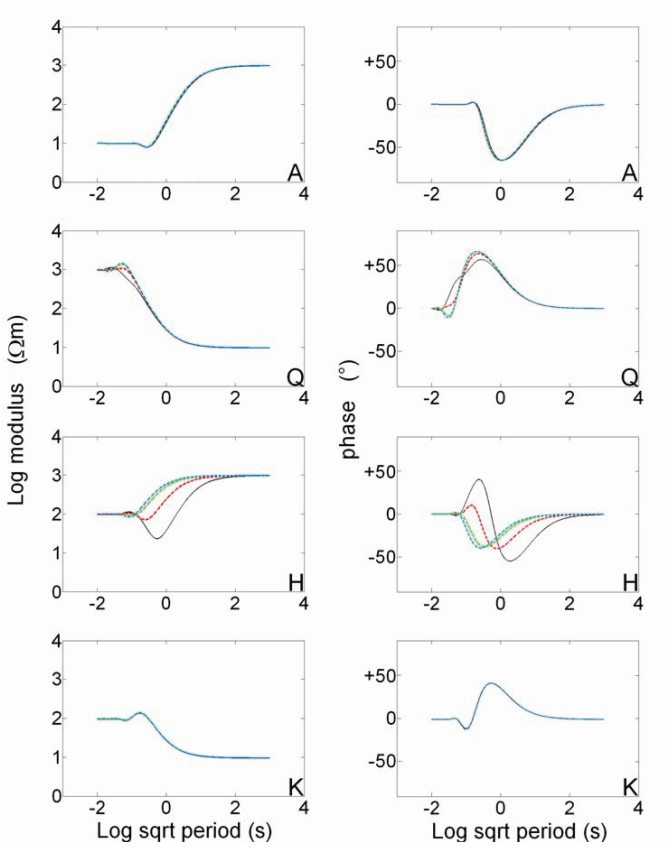

Figure 3c. MT apparent impedivity modulus and phase simulated responses for the A, Q, H and K three-layer sequences of Fig. 1, with the second layer affected by a Cole-Cole type non-resonant negative dispersion. The black lines are the reference not dispersive MT responses. The flatting factor and principal time constant are fixed, respectively $c_- = 0.75$ and $\tau_- = 100\,\mathrm{s}$, while the negative dispersion amplitude is variable with values $m_- = -9$ (red lines), $m_- = -99$ (green lines) and $m_- = -999$ (blue lines).

out within the dispersive layer, and on how much part of the dispersion frequency band falls within this MT window. This explains why the A, Q and K curves do not show remarkable IP effects.

3.2. The MT Response with Non-resonant Negative Dispersion

Referring to the Cole-Cole type non-resonant negative dispersion model given in Eq. (6), the simulations have again been done by fixing two of

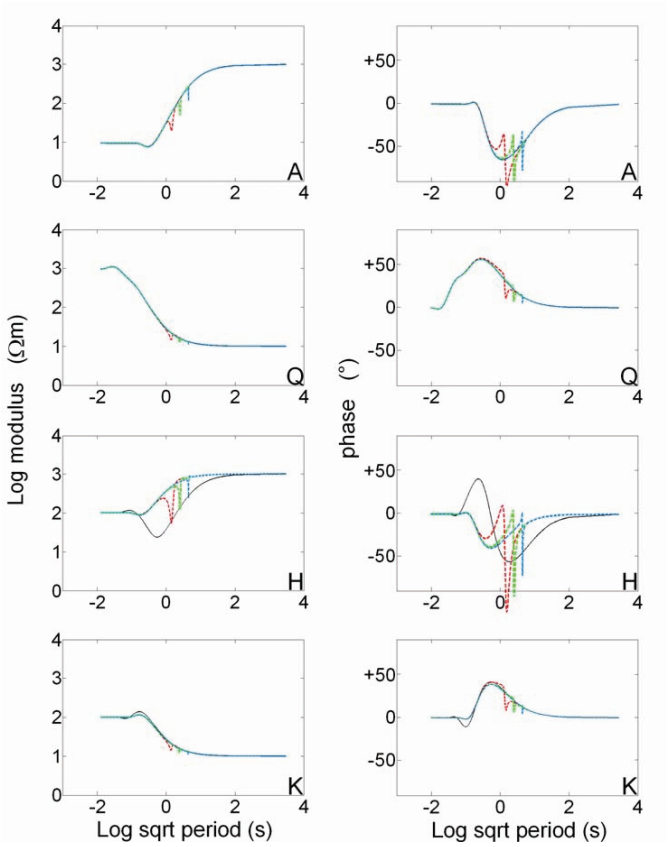

Figure 4a. MT apparent impedivity modulus and phase simulated responses for the A, Q, H and K three-layer sequences of Fig. 1, with the second layer affected by a resonant flat dispersion. The black lines are the reference not dispersive MT responses. Fixed parameters are $\sigma_2 = 0.1\,\mathrm{S/m}$ and $\gamma_2 = 10\,\mathrm{Hz}$, while the variable parameter is $\lambda_2 = 1\,\mathrm{s}$ (red lines), $\lambda_2 = 10\,\mathrm{s}$ (green lines) and $\lambda_2 = 100\,\mathrm{s}$ (blue lines).

the three dispersion parameters c_-, m_- and τ_- and letting the third vary. The following three sets of simulations have thus been drawn:

1st set: $c_- = 0.75$, $m_- = -999$ and $\tau_- = 1$, 10, 100 s, (Fig. 3(a)),

2nd set: $m_- = -999$, $\tau_- = 100$ s and $c_- = 0.25$, 0.5, 0.75, (Fig. 3(b)),

3rd set: $c_- = 0.75$, $\tau_- = 100$ s and $m_- = -9$, -99, -999, (Fig. 3(c)).

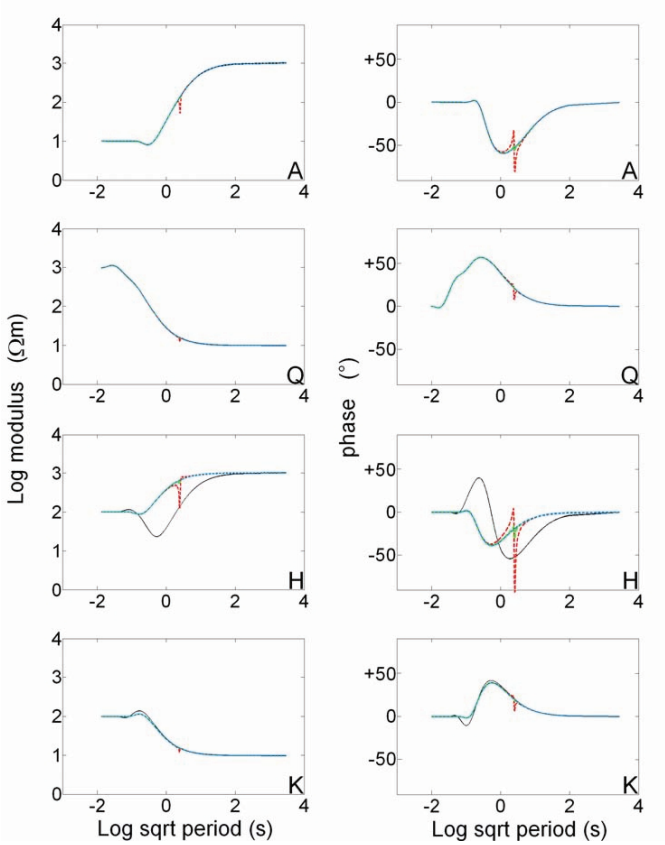

Figure 4b. MT apparent impedivity modulus and phase simulated responses for the A, Q, H and K three-layer sequences of Fig. 1, with the second layer affected by a resonant flat dispersion. The black lines are the reference not dispersive MT responses. Fixed parameters are $\gamma_2 = 10$ Hz and $\lambda_2 = 10$ s, while the variable parameter is $\sigma_2 = 0.1$ S/m (red lines), $\sigma_2 = 0.01$ S/m (green lines) and $\sigma_2 = 0.001$ S/m (blue lines).

Figure 3(a) shows again a quite imperceptible influence of τ_-. The blue, red and green curves are still overlapping, except for the H type section.

The same elusive effects are also produced by changing c_- (Fig. 3(b)) and m_- (Fig. 3(c)), except again for the H type section, which appears the most responsive section also to this dispersion typology.

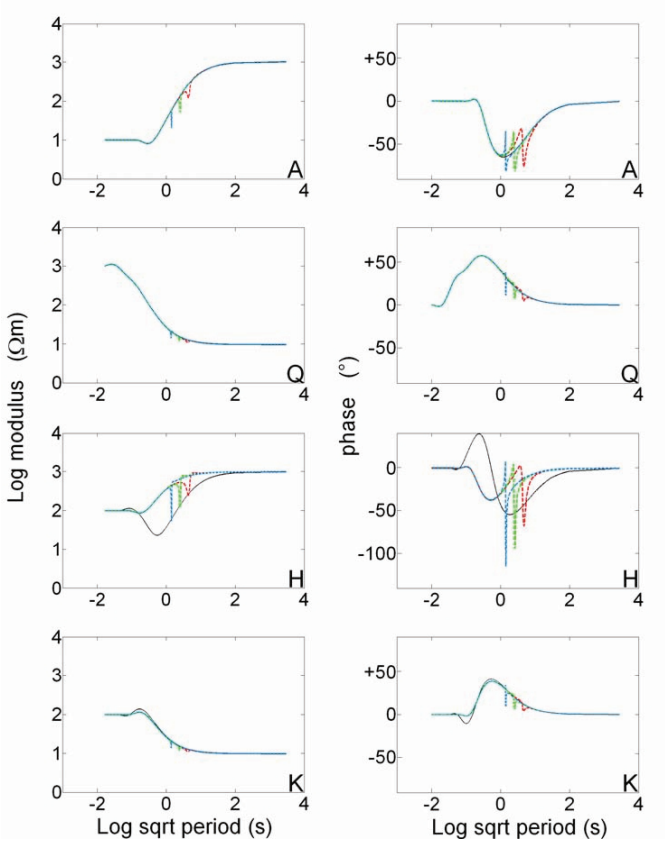

Figure 4c. MT apparent impedivity modulus and phase simulated responses for the A, Q, H and K three-layer sequences of Fig. 1, with the second layer affected by a resonant flat dispersion. The black lines are the reference not dispersive MT responses. Fixed parameters are $\sigma_2 = 0.1\,\mathrm{S/m}$ and $\lambda_2 = 10\,\mathrm{s}$, while the variable parameter is $\gamma_2 = 1\,\mathrm{Hz}$ (red lines), $\gamma_2 = 10\,\mathrm{Hz}$ (green lines) and $\gamma_2 = 100\,\mathrm{Hz}$ (blue lines).

3.3. The MT Response with Resonant Flat Dispersion

Simulations have been calculated using the following sets of dispersion parameters:

1st set: $\sigma_2 = 0.1\,\mathrm{S/m}$, $\gamma_2 = 10\,\mathrm{Hz}$, $\lambda_2 = 1, 10, 100\,\mathrm{s}$, (Fig. 4(a)),

2nd set: $\gamma_2 = 10\,\mathrm{Hz}$, $\lambda_2 = 10\,\mathrm{s}$, $\sigma_2 = 0.1, 0.01, 0.001\,\mathrm{S/m}$, (Fig. 4(b)),

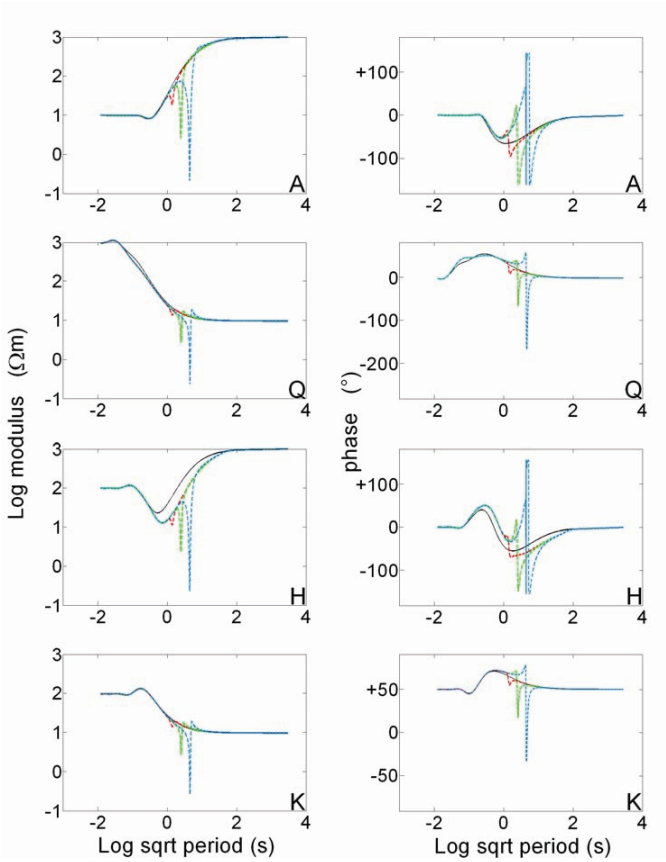

Figure 5a. MT apparent impedivity modulus and phase simulated responses for the A, Q, H and K three-layer sequences of Fig. 1, with the second layer affected by a resonant positive dispersion. The black lines are the reference dispersion-free responses. The positive dispersion amplitude, flatting factor and time constant parameters are $m_+ = 0.5$, $c_+ = 1$ and $\tau_+ = 1000\,\mathrm{s}$, respectively. Fixed are also $\sigma_3 = 0.1\,\mathrm{S/m}$ and $\gamma_3 = 10\,\mathrm{Hz}$, while the variable parameter is $\lambda_3 = 1\,\mathrm{s}$ (red lines), $\lambda_3 = 10\,\mathrm{s}$ (green lines) and $\lambda_3 = 100\,\mathrm{s}$ (blue lines).

3rd set: $\sigma_2 = 0.1\,\mathrm{S/m}$, $\lambda_2 = 10\,\mathrm{s}$, $\gamma_2 = 1$, 10, 100 Hz, (Fig. 4(c)). The reference formula is given in Eq. (7).

As previously, also the resonant flat dispersion effect can hardly be detected in the A, Q and K curves drawn in Figs. 4(a), 4(b) and 4(c), except for the H section, where huge resonance peaks and curve distortions emerge.

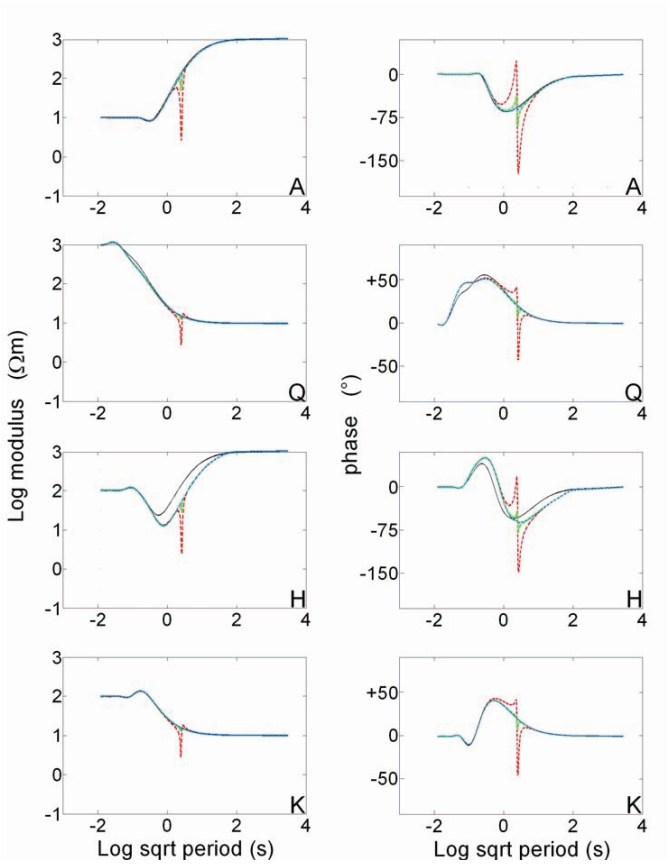

Figure 5b. MT apparent impedivity modulus and phase simulated responses for the A, Q, H and K three-layer sequences of Fig. 1, with the second layer affected by a resonant positive dispersion. The black lines are the reference dispersion-free MT responses. The positive dispersion amplitude, flatting factor and time constant parameters are $m_+ = 0.5$, $c_+ = 1$ and $\tau_+ = 1000\,\mathrm{s}$, respectively. Fixed are also $\gamma_3 = 10\,\mathrm{Hz}$ and $\lambda_3 = 10\,\mathrm{s}$, whereas the variable parameter is $\sigma_3 = 0.1\,\mathrm{S/m}$ (red lines), $\sigma_3 = 0.01\,\mathrm{S/m}$ (green lines) and $\sigma_3 = 0.001\,\mathrm{S/m}$ (blue lines).

3.4. The MT Response with Resonant Positive Dispersion

Simulations have been done using the following sets of resonant positive dispersion parameters:

1st set: $m_+ = 0.5$, $c_+ = 1$, $\tau_+ = 1000\,\mathrm{s}$, $\sigma_3 = 0.1\,\mathrm{S/m}$, $\gamma_3 = 10\,\mathrm{Hz}$, $\lambda_3 = 1,\ 10,\ 100\,\mathrm{s}$, (Fig. 5(a)),

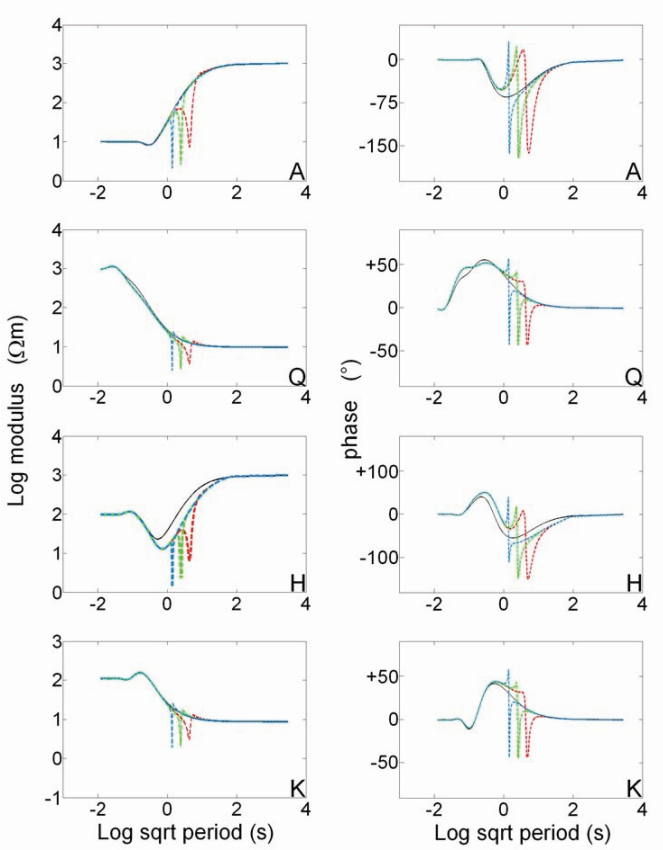

Figure 5c. MT apparent impedivity modulus and phase simulated responses for the A, Q, H and K three-layer sequences of Fig. 1, with the second layer affected by a resonant positive dispersion. The black lines are the reference dispersion-free MT responses. The positive dispersion amplitude, flatting factor and time constant parameters are $m_+ = 0.5$, $c_+ = 1$ and $\tau_+ = 1000\,\mathrm{s}$, respectively. Fixed are also $\sigma_3 = 0.1\,\mathrm{S/m}$ and $\lambda_3 = 10\,\mathrm{s}$, while the variable parameter is $\gamma_3 = 1\,\mathrm{Hz}$ (red lines), $\gamma_3 = 10\,\mathrm{Hz}$ (green lines) and $\gamma_3 = 100\,\mathrm{Hz}$ (blue lines).

2nd set: $m_+ = 0.5$, $c_+ = 1$, $\tau_+ = 1000\,\mathrm{s}$, $\gamma_3 = 10\,\mathrm{Hz}$, $\lambda_3 = 10\,\mathrm{s}$, $\sigma_3 = 0.1$, 0.01, 0.001 S/m, (Fig. 5(b)),

3rd set: $m_+ = 0.5$, $c_+ = 1$, $\tau_+ = 1000\,\mathrm{s}$, $\sigma_3 = 0.1\,\mathrm{S/m}$, $\lambda_3 = 10\,\mathrm{s}$, $\gamma_3 = 1$, 10, 100 Hz, (Fig. 5(c)).

The reference formula is given in Eq. (8). For the first time, in all of the type sections MT is able to detect the dispersion effect. In fact,

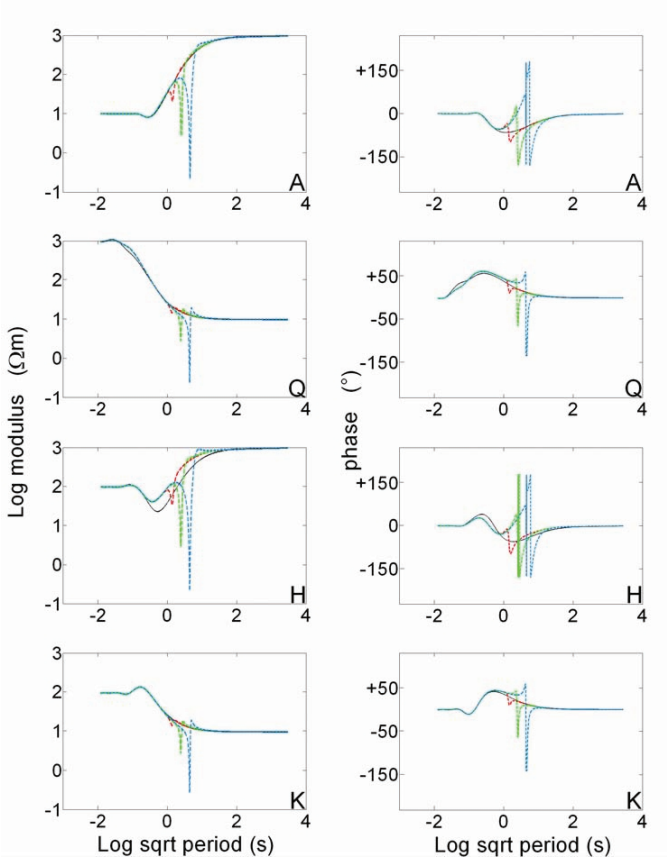

Figure 6a. MT apparent impedivity simulated responses for the A, Q, H and K three-layer sequences of Fig. 1, with the second layer affected by a resonant negative dispersion. The black lines are the reference dispersion-free MT curves. The negative dispersion amplitude, flatting factor and time constant are $m_- = -1$, $c_- = 1$ and $\tau_- = 500\,\mathrm{s}$, respectively. Fixed are also $\sigma_3 = 0.1\,\mathrm{S/m}$ and $\gamma_3 = 10\,\mathrm{Hz}$, while the variable parameter is $\lambda_3 = 1\,\mathrm{s}$ (red lines), $\lambda_3 = 10\,\mathrm{s}$ (green lines) and $\lambda_3 = 100\,\mathrm{s}$ (blue lines).

quite evident resonance peaks always appear, with a slight but well outlined full curve distortion only in the H section. As it can easily be observed in Fig. 5(b), the peak is strongly regulated by the resonance conductivity σ_3, in the sense that the larger the σ_3 the larger the amplitude. It is worth outlining that the position and/or the amplitude of the peak appear always well distinguishable, independently of the

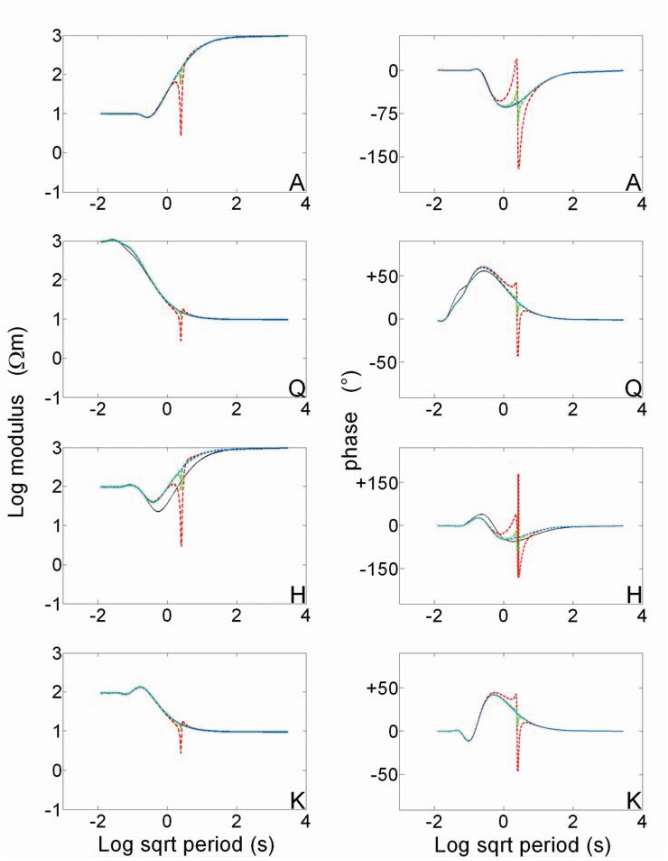

Figure 6b. MT apparent impedivity simulated responses for the A, Q, H and K three-layer sequences of Fig. 1, with the second layer affected by a resonant negative dispersion. The black lines are the reference dispersion-free MT curves. The negative dispersion amplitude, flatting factor and time constant are $m_- = -1$, $c_- = 1$ and $\tau_- = 500\,\mathrm{s}$, respectively. Fixed are also $\gamma_3 = 10\,\mathrm{Hz}$ and $\lambda_3 = 10\,\mathrm{s}$, while the variable parameter is $\sigma_3 = 0.1\,\mathrm{S/m}$ (red lines), $\sigma_3 = 0.01\,\mathrm{S/m}$ (green lines) and $\sigma_3 = 0.001\,\mathrm{S/m}$ (blue lines).

choice of the parameters which regulate the resonance part of the dispersion model.

3.5. The MT Response with Resonant Negative Dispersion

Simulations have been done using the following sets of parameters:

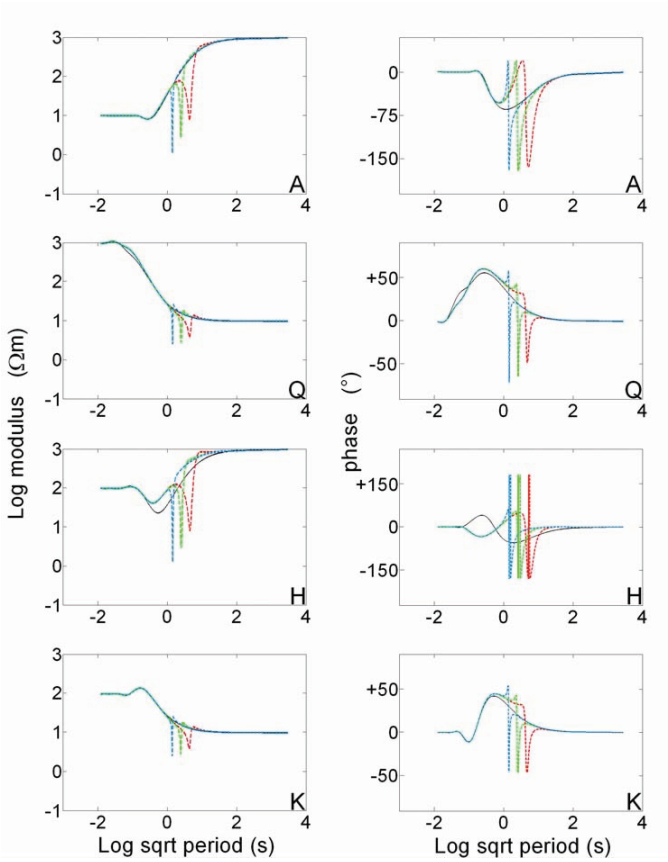

Figure 6c. MT apparent impedivity simulated responses for the A, Q, H and K three-layer sequences of Fig. 1, with the second layer affected by a resonant negative dispersion. The black lines are the reference dispersion-free MT curves. The negative dispersion amplitude, flatting factor and time constant are $m_- = -1$, $c_- = 1$ and $\tau_- = 500\,\mathrm{s}$, respectively. Fixed are also $\sigma_3 = 0.1\,\mathrm{S/m}$ and $\lambda_3 = 10\,\mathrm{s}$, while the variable parameter is $\gamma_3 = 1\,\mathrm{Hz}$ (red lines), $\gamma_3 = 10\,\mathrm{Hz}$ (green lines) and $\gamma_3 = 100\,\mathrm{Hz}$ (blue lines).

1st set: $m_- = -1$, $c_- = 1$, $\tau_- = 500\,\mathrm{s}$, $\sigma_3 = 0.1\,\mathrm{S/m}$, $\gamma_3 = 10\,\mathrm{Hz}$, $\lambda_3 = 1,\ 10,\ 100\,\mathrm{s}$, (Fig. 6(a)),

2nd set: $m_- = -1$, $c_- = 1$, $\tau_- = 500\,\mathrm{s}$, $\gamma_3 = 10\,\mathrm{Hz}$, $\lambda_3 = 10\,\mathrm{s}$, $\sigma_3 = 0.1,\ 0.01,\ 0.001\,\mathrm{S/m}$, (Fig. 6(b)),

3rd set: $m_- = -1$, $c_- = 1$, $\tau_- = 500\,\mathrm{s}$, $\sigma_3 = 0.1\,\mathrm{S/m}$, $\lambda_3 = 10\,\mathrm{s}$, $\gamma_3 = 1,\ 10,\ 100\,\mathrm{Hz}$, (Fig. 6(c)).

There is no general comment to add to what has already been said previously as to the influence of the resonant addendum in the dispersion model. Identical effects are in fact noted, except for the inverted behavior of the non-resonant part, which is detectable, as usual, only in the H-type three-layer section.

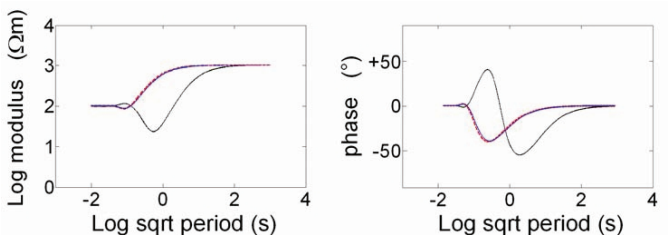

Figure 7. MT equivalence between a dispersive H-type three-layer model and a not dispersive two-layer model. The black lines are the reference apparent impedivity modulus and phase curves for the dispersion-free H-type model drawn in Fig. 1 The red lines are the apparent impedivity modulus and phase responses for the same H-type sequence, with the second layer affected by a non-resonant negative dispersion, with parameters $m_- = -999$, $c_- = 1$ and $\tau_- = 100\,\mathrm{s}$. The blue lines are the corresponding curves for the dispersion-free two-layer sequence with $\rho_1 = 100\,\Omega\mathrm{m}$, $\rho_2 = 1000\,\Omega\mathrm{m}$ and $t_1 = 500\,\mathrm{m}$.

4. CONCLUSIONS

We have shown in this paper how the electric dispersion phenomenology can affect the MT response. A three-layer earth section has been adopted to simplify the analysis. Mostly important have been the results achieved for an H-type section, where the dispersion phenomenology within the sandwiched layer shows its most pronounced effects.

It is worth stressing again that the H-type layer sequence has been shown to be the most recurrent model, fitting the MT spectrum in oil and geothermal exploration [28, 42]. In fact, as mentioned in the introduction, strong dispersion phenomena may occur in a permeable rock, underlying a cover layer, because of the diffuse presence of mineral

and clay particles formed by the aggressive action of uprising fluids from a subjacent reservoir. The electric properties of such a layered sequence can likely be condensed into an H-type sequence. In fact, the larger is the amount of the alteration particles, which are deposited in the fractured layer, the higher is its conductivity, well over that of the cover layer. Furthermore, exploited dense oilfields, gas- and vapor-dominated reservoirs have largely been proved to be identified by a DC resistivity much higher than that of the overlying altered layer. Thus, in conclusion, the MT dispersive method can likely have some good chances to be a powerful large-scale mapping tool of the electrical properties of rocks, in the search for earth's energy resources underground.

It is equally important to point out also the misleading implications one may incur if the dispersion phenomenon is not taken into account in the interpretation phase of the MT sounding curves. It has, in fact, been shown that, when the dispersion effects on the MT curves do not cause any apparent incompatibility with the MT theory over layered structures, a dispersive MT response can as well be interpreted as a non-dispersive one. Fig. 7 shows a clear example of such an occurrence. A three-layer H-type model, affected by a non-resonant negative dispersion, can equally well be interpreted as a dispersion-free two layer sequence.

Of course, we have not made an exhaustive study of all the possible MT dispersive responses, having limited our attention to the large-scale 1D assumption. Now that advanced 2D and 3D modeling and inversion tools are available [2], a good challenge will be the small-scale analysis of the distortions provoked by dispersion in both vertically and laterally confined structures. This new approach will make MT a more efficient tool to explore deep crustal structures with an enhanced relative resolution power, comparable with that of near-surface methods, like GPR [13, 22, 32, 38, 39], and shallow-depth methods, like geoelectrics and magnetics [16–18].

REFERENCES

1. Ageev, V. V. and B. S. Svetov, "The influence of rock polarizability on electromagnetic soundings," *Izvestia RAS, Physics of the Solid Earth*, Vol. 35, 16–24, 1999.
2. Avdeev, D. B. and A. D. Avdeeva, "A rigorous three-dimensional magnetotelluric inversion," *Progress In Electromagnetics Research*, PIER 62, 41–48, 2006.
3. Balanis, C. A., *Advanced Engineering Electromagnetics*, J. Wiley & Sons, New York, 1989.

4. Bertin, J. and J. Loeb, *Experimental and Theoretical Aspects of Induced Polarization*, Gebrüder-Bornträger, Berlin, 1976.
5. Cole, K. S. and R. H. Cole, "Dispersion and absorption in dielectrics," *J. Chem. Phys.*, Vol. 9, 341–351, 1941.
6. Coppola, B., R. Di Maio, I. Marini, A. Merla, D. Patella, G. Pulelli, F. M. Rossi, and A. Siniscalchi, "Study of the Simplon area geothermal anomaly in the frame of a transalpine deep railway tunnel feasibility project," *Underground Transportation Infrastructures*, J. L. Reith (ed.), 93–102, Balkema, Rotterdam, 1993.
7. Debye, P., *Polar Molecules*, Chemical Catalogue Company, New York, 1928.
8. Di Maio, R., D. Patella, and A. Siniscalchi, "Sul problema del riconoscimento di uno strato elettricamente polarizzabile mediante misure magnetotelluriche," *Atti del II Convegno di Geomagnetismo ed Aeronomia*, A. Meloni and B. Zolesi (ed.), 239–250, Istituto Nazionale di Geofisica e Vulcanologia, Roma, 1991.
9. Di Maio, R., P. Mauriello, D. Patella, Z. Petrillo, S. Piscitelli, A. Siniscalchi, and M. Veneruso, "Self-potential, geoelectric and magnetotelluric studies in Italian active volcanic areas," *Ann. Geofis.*, Vol. 40, 519–537, 1997.
10. Di Maio, R., D. Patella, Z. Petrillo, A. Siniscalchi, G. Cecere, and P. de Martino, "Application of electric and electromagnetic methods to the study of the Phlegrean Fields caldera," *Ann. Geofis.*, Vol. 43, 375-390, 2000.
11. Fink, J. B., E. O. McAlister, B. K. Sternberg, W. G. Wieduwilt, and S. H. Ward, *Induced Polarization: Applications and Case Histories*, Investigations in Geophysics, Vol. 4, Society of Exploration Geophysicists, Tulsa, Oklahoma, 1990.
12. Giammetti, S., D. Patella, A. Siniscalchi, and A. Tramacere, "The Siena Graben: Combined interpretation of DES and MT soundings," *Ann. Geofis.*, Vol. 39, 189–200, 1996.
13. Ivashov, S. I., I. A. Vasiliev, T. D. Bechtel, and C. Snapp, "Comparison between impulse and holographic subsurface radar for NDT of space vehicle structural materials," *Progress In Electromagnetics Research Online*, Vol. 3, 658–661, 2007.
14. Kaufman, A. A. and G. V. Keller, *The Magnetotelluric Sounding Method*, Elsevier, Amsterdam, 1981.
15. Manzanares-Martinez, J. and J. Gaspar-Armenta, "Direct integration of the constitutive relations for modelling dispersive metamaterials using the finite difference time-domain technique,"

Journal of Electromagnetic Waves and Applications, Vol. 21, 2297–2310, 2007.

16. Mauriello, P. and D. Patella, "Localization of magnetic sources underground by a probability tomography approach," *Progress In Electromagnetics Research M*, Vol. 3, 27–56, 2008.
17. Mauriello, P. and D. Patella, "Resistivity tensor probability tomography," *Progress In Electromagnetics Research B*, Vol. 8, 129–146, 2008.
18. Mauriello, P. and D. Patella, "Geoelectrical anomalies imaged by polar and dipolar probability tomography," *Progress In Electromagnetics Research*, PIER 87, 63–88, 2008.
19. Mauriello, P., D. Patella, and A. Siniscalchi, "The magnetotelluric response over two-dimensional media with resistivity frequency dispersion," *Geophys. Prosp.*, Vol. 44, 789–818, 1996.
20. Mauriello, P., D. Patella, Z. Petrillo, and A. Siniscalchi, "An integrated magnetotelluric study of the Mt. Etna volcanic structur," *Ann. Geofis.*, Vol. 43, 325–342, 2000.
21. Mauriello, P., D. Patella, Z. Petrillo, A. Siniscalchi, T. Iuliano, and C. Del Negro, "A geophysical study of the Mount Etna volcanic area," *Mt. Etna: Volcano Laboratory*, A. Bonaccorso, S. Calvari, M. Coltelli, C. Del Negro, and S. Falsaperla (eds.), Vol. 143, 273–291, American Geophysical Union, Geophysical Monograph Series, 2004.
22. Nishimoto, M., S. Ueno, and Y. Kimura, "Feature extraction from GPR data for identification of landmine-like objects under rough ground surface," *Journal of Electromagnetic Waves and Applications*, Vol. 20, 1577–1586, 2006.
23. Patella, D., "Tutorial: Interpretation of magnetotelluric measurements over an electrically dispersive one-dimensional earth," *Geophys. Prosp.*, Vol. 35, 1–11, 1987.
24. Patella, D., "I principi metodologici della magnetotellurica su mezzi generalmente dispersivi," *Ann. Geofis.*, Vol. 36, 147–160, 1993.
25. Patella, D., "On the role of the J-E constitutive relationship in applied geoelectromagnetism," *Ann. Geophys.*, Vol. 46, 589–597, 2003.
26. Patella, D., "Modelling electrical dispersion phenomena in earth materials," *Ann. Geophys.*, Vol. 51, 2008.
27. Patella, D., A. Tramacere, R. Di Maio, and A. Siniscalchi, "Experimental evidence of resistivity frequency-dispersion in magnetotellurics in the Newberry (Oregon), Snake River Plain

(Idaho) and Campi Flegrei (Italy) volcano-geothermal areas," *J. Volcanol. Geoth. Res.*, Vol. 48, 61–75, 1991.

28. Pellerin, L., J. M. Johnston, and G. W. Hohmann, "A numerical evaluation of electromagnetic methods in geothermal exploration," *Geophysics*, Vol. 61, 121–137, 1996.
29. Pelton, W. H., S. H. Ward, P. G. Hallof, W. R. Sill, and P. H. Nelson, "Mineral discrimination and removal of inductive coupling with multi-frequency IP," *Geophysics*, Vol. 43, 588–603, 1978.
30. Pelton, W. H., W. R. Sill, and B. D. Smith, "Interpretation of complex resistivity and dielectric data, Part I," *Geophys. Trans.*, Vol. 29, 297–330, 1983.
31. Prosvirnin, S. L. and S. Zouhdi, "On the effective constitutive parameters of metal-dielectric arrays of complex-shaped particles," *Journal of Electromagnetic Waves and Applications*, Vol. 20, 583–598, 2006.
32. Razevig, V. V., S. I. Ivashov, A. P. Sheyko, I. A. Vasilyev, and A. V. Zhuravlev, "An example of holographic radar using at restoration works of historical building," *Progress In Electromagnetics Research Letters*, Vol. 1, 173–179, 2008.
33. Seigel, H. O., "Mathematical formulation and type curves for induced polarization," *Geophysics*, Vol. 24, 547–565, 1959.
34. Sjöberg, D., "Exact and asymptotic dispersion relations for homogenization of stratified media with two phases," *Journal of Electromagnetic Waves and Applications*, Vol. 20, 781–792, 2006.
35. Stoyer, C. H., "Consequences of induced polarization in magnetotelluric interpretation," *Pure and Appl. Geophys.*, Vol. 114, 435–449, 1976.
36. Sumner, J. S., *Principles of Induced Polarization for Geophysical Exploration*, Elsevier, Amsterdam, 1976.
37. Svetov, B. S. and V. V. Ageev, "High resolution electromagnetic methods and low frequency dispersion of rock conductivity," *Ann. Geofis.*, Vol. 42, 699–713, 1999.
38. Uduwawala, D., "Modeling and investigation of planar parabolic dipoles for GPR applications: A comparison with bow-tie using FDTD," *Journal of Electromagnetic Waves and Applications*, Vol. 20, 227–236, 2006.
39. Van den Bosch, I., S. Lambot, M. Acheroy, I. Huynen, and P. Druyts, "Accurate and efficient modelling of monostatic GPR signal of dielectric targets buried in stratified media," *Journal of Electromagnetic Waves and Applications*, Vol. 20, 283–290, 2006.

40. Wait, J. R., *Overvoltage Research and Geophysical Applications,* Pergamon, Oxford, 1959.
41. Wait, J. R., *Geo-electromagnetism*, Academic Press, New York, 1982.
42. Zhdanov, M. S. and G. V. Keller, *The Geoelectrical Methods in Geophysical Exploration*, Elsevier, Amsterdam, 1994.